Saddle-node bifurcations in the spectrum of HOCl

J. Weiß, J. Hauschildt, S. Yu. Grebenshchikov, R. Düren, and R. Schinke[a)]
Max-Planck-Institut für Strömungsforschung, D-37073 Göttingen, Germany

J. Koput
Department of Chemistry, Adam Mickiewicz University, 60-780 Poznań, Poland

S. Stamatiadis and S. C. Farantos
*Institute of Electronic Structure and Laser Foundation for Research and Technology, Hellas, Greece
and Department of Chemistry, University of Crete, Iraklion 711 10, Crete, Greece*

A detailed analysis of the bound-state spectrum of HOCl (hypoclorous acid) in the ground electronic state is presented. Exact quantum mechanical calculations (filter diagonalization) are performed employing an *ab initio* potential energy surface, which has been constructed using the multireference configuration-interaction method and a quintuple-zeta one-particle basis set. The wave functions of all bound states up to the HO+Cl dissociation threshold are visually inspected in order to assign the spectrum in a rigorous way and to elucidate how the spectrum develops with energy. The dominant features are (1) a 2:1 anharmonic resonance between the bending mode and the OCl stretching mode, which is gradually tuned in as the energy increases, and (2) a saddle-node bifurcation, i.e., the sudden birth of a new family of states. The bifurcation is further investigated in terms of the structure of the classical phase space (periodic orbits, continuation/bifurcation diagram). It is also discussed how the spectrum of bound states persists into the continuum and how the various types of quantum mechanical continuum wave functions affect the state-specific dissociation rates. © *2000 American Institute of Physics.* [S0021-9606(99)00901-0]

I. INTRODUCTION

The spectrum of vibrational states of a molecule reflects in a unique way the intramolecular forces.[1] It is usually regular and easily assignable in terms of a set of quantum numbers, provided the excitation energy is not too high, i.e., the displacements of the vibrational coordinates from equilibrium are small.[2] With increasing energy the coupling between the modes typically grows with the consequence that the spectrum becomes more complex and the assignment of the states gradually becomes more difficult.[3] Eventually the dynamics is mainly irregular and the majority of states cannot be straightforwardly labeled by quantum numbers. The ''rate'' with which this change occurs depends, of course, on the particular molecule, i.e., the potential energy surface (PES) and the masses of the constituent atoms.

As one climbs up the ladder of vibrational energies, interesting effects may occur.[4] A common effect is the existence of an anharmonic resonance — the near degeneracy of vibrational levels, which leads to a substantial mixing of the corresponding (zero-order) basis functions.[5–9] As a result of such resonances the energy levels are grouped into polyads. Examples, which have been recently investigated in some detail by us, include the 1:1 DC stretch:CO stretch resonance in DCO,[10] the 1:1 NO stretch:HNO bend resonance in HNO,[11] and the 1:2 HCP bend:CP stretch resonance in HCP.[12,13] In all these examples the resonances are already present in the fundamentals and continue to shape the spectrum up to high energies. Another possibility is that two

frequencies gradually tune into resonance as the energy increases, because one mode is considerably more anharmonic than the other one. The result is that the mixing between the modes gradually develops with energy and becomes fully established at relatively high energies. An example, which will be investigated in the present study, is the 2:1 HOCl bend:OCl stretch resonance in HOCl.

Anharmonic resonances bring about intriguing effects as one follows the spectrum from low to high energies, e.g., the birth of a completely new class of wave functions, which did not exist at lower energies. Such an effect, known as saddle-node or tangent bifurcation in the nonlinear dynamics literature,[14,15] has been predicted to happen in HCP[12] and indeed has been observed in stimulated emission pumping (SEP) spectra.[13,16] As we will demonstrate in the present work a similar bifurcation exists in HOCl.

Understanding the structure of a quantum mechanical spectrum over an extended energy regime can be quite cumbersome, even for a triatomic molecule. However, in numerous applications it has been demonstrated that classical mechanics, especially periodic orbits[17,18] and continuation/bifurcation diagrams,[19] can be extremely helpful in interpreting quantum spectra. This has been shown for HCP[12] and it is likewise true for HOCl.

The bound states of a molecule do not abruptly terminate at the dissociation threshold, but persist into the continuum as resonance or quasibound states.[20] While bound states are the real poles of the Green's function, resonances are poles in the complex energy plane with the imaginary parts representing the dissociation rates or the inverse of the lifetimes.

[a)]Electronic mail: rschink@gwdg.de

The decay of resonance states is intimately related to unimolecular dissociation processes.[21,22] Whether a resonance state decays slowly or fast ultimately depends on the structure of the corresponding wave function. In a recent article we found that at threshold the dissociation rate of HOCl varies by more than seven orders of magnitude.[23] In the present article we attempt to rationalize this ''unexpectedly broad'' distribution of resonance widths in terms of the nature of the wave functions near the HO+Cl threshold.

The spectroscopy[24,25] and dissociation[26–28] of HOCl are the target of recent experimental interest. However, due to experimental limitations (vibrational overtone spectroscopy) only states in the vicinity of overtones of the HO bond are considered — out of the ~800 bound states merely 2%–3% have been experimentally analyzed. Parallel to our own theoretical work, the spectroscopy and dissociation of HOCl is currently under investigation — using an independently calculated *ab initio* PES — by Skokov and co-workers.[29–32] We will refer to their work in the following when it is appropriate.

The subject of the present article is a comprehensive analysis of the HOCl spectrum from the bottom of the potential well to the HO+Cl dissociation threshold and above. We will focus the discussion on (i) how the level pattern and the underlying wave functions change with energy, (ii) how new states appear as a consequence of a saddle-node bifurcation of the classical phase space, and (iii) how the structure of the bound-state spectrum affects the state-specific dissociation rates. The article is organized in the following way: The *ab initio* calculations and the analytical fit of the PES will be described in Sec. II, followed by a brief account of the dynamics calculations in Sec. III. The evolution of the bound states is the topic of Sec. IV, followed by classical calculations in Sec. V, which elucidate the gross features of the quantum spectrum in terms of a continuation/bifurcation diagram. The consequences of the various types of wave functions for the dissociation rates are explicated in Sec. VI. The main results are summarized in Sec. VII. In a future paper we will provide a more detailed analysis of the bound-state structure in terms of a two-dimensional (2D) model, in which the HO stretching degree of freedom is adiabatically separated.[33] The reduction to two degrees of freedom allows a more detailed analysis of the variation of the classical phase space with energy and the classical/quantum mechanical correspondence. Additional clues about the spectrum of HOCl are obtained from a description in terms of a 1:2 resonance Hamiltonian model, fitted to either the 2D or the three-dimensional (3D) quantum mechanical energy level spectrum.[33]

II. POTENTIAL ENERGY SURFACE

A. *Ab initio* calculations

The total energies of hypochlorous acid are calculated using the internally contracted multireference configuration interaction method, icMRCI.[34,35] The one-particle basis set employed in this study is the correlation-consistent polarized basis set of quintuple-zeta quality, cc-pV5Z.[36,37] The cc-pV5Z basis set consists of a $(20s12p4d3f2g1h)/$

$[7s6p4d3f2g1h]$ set for chlorine, a $(14s8p4d3f2g1h)/$ $[6s5p4d3f2g1h]$ set for oxygen, and a $(8s4p3d2f1g)/$ $[5s4p3d2f1g]$ set for hydrogen, thus resulting in a molecular one-particle basis set of 241 contracted functions. Only the spherical harmonic components of the d through h polarization functions are used. The reference wave function in the icMRCI calculations consists of a full valence complete active space (CAS). The wave function thus includes all excitations of 14 valence electrons in 9 molecular orbitals corresponding to the valence atomic sp orbitals of chlorine and oxygen, and the $1s$ orbital of hydrogen. For each point of the PES, the reference wave function is determined in the complete active space self-consistent field calculation (CASSCF).[38,39] The molecular $1s$- and $2sp$-like core orbitals of chlorine and the $1s$-like core orbital of oxygen are kept doubly occupied in all the configurations and optimized. In the vicinity of the minimum of the PES, the CI-expansion coefficient of the SCF configuration in the CASSCF wave function is determined to be about 0.98 and there are only two excited configurations with coefficients greater than 0.05. The total energy of hypochlorous acid is determined in the following icMRCI calculation, in which all single and double excitations with respect to the reference wave function are included and external configurations are internally contracted.[34,35] The molecular core orbitals are kept doubly occupied in all the configurations. This results in over one million contracted configurations (in contrast to over 75 million uncontracted configurations). The multireference Davidson correction[40,41] to the calculated energy (icMRCI+Q) is then employed to approximately account for the effects of higher excitations. The total energies are determined to an accuracy better than 10^{-8} hartree. The calculations are performed using the MOLPRO-96 program.[42]

B. Analytical fit

The PES is constructed by varying the two bond distances R_{HO} and R_{OCl} and the HOCl bond angle α on a three-dimensional grid: $2.5a_0 \leq R_{OCl} \leq 9a_0$, $1.3a_0 \leq R_{HO} \leq 3.5a_0$, and $20° \leq \alpha \leq 160°$. The grid spacings are $\Delta R_{OCl} = \Delta R_{HO} = 0.1a_0$, and $\Delta \alpha = 10°$ for the largest part of the grid. Near the equilibrium smaller spacings are chosen, whereas for large OCl distances the grid is coarser. Altogether we have calculated 1234 points. Only the HO+Cl exit channel is sampled; the other two dissociation channels, O+HCl and H+OCl,[43,44] are energetically considerably higher and therefore not considered in the present work.

The analytical fit expression uses the three bond distances R_{HO}, R_{OCl}, and R_{ClH} rather than the two bond distances and the HOCl bond angle. It is hoped that this gives a more reasonable extrapolation to the two linear configurations ($\alpha = 0°$ and $180°$, where no *ab initio* points have been calculated). Following Sorbie and Murrell[45] the total potential is written as

$$V(R_{OCl}, R_{HO}, R_{ClH}) = V_I(R_{OCl}, R_{HO}, R_{ClH}) + v_{HO}(R_{HO}),$$
(1)

with V_I going to zero for large OCl bond distances. Because of some numerical instabilities of the *ab initio* calculations at

large OCl distances, we do not calculate the asymptotic HO oscillator, but use instead the Morse expression for it,

$$v_{HO}(R_{HO}) = D_{HO}[1 - e^{-\beta_{HO}(R_{HO} - R_{HO}^e)}]^2. \quad (2)$$

The parameters are taken from the literature:[46] $D_{HO} = 4.621$ eV, $\beta_{HO} = 1.2139 a_0^{-1}$, and $R_{HO}^e = 1.8323 a_0$. In what follows, energy normalization is such that $E = 0$ corresponds to HO+Cl with the HO distance fixed at equilibrium. The ''interaction potential'' is written as a threefold sum of one-dimensional functions,

$$V_I(R_{OCl}, R_{HO}, R_{ClH})$$

$$= \tfrac{1}{2}[1 + \tanh(6 - R_{OCl})]$$

$$\times \sum_{i=0}^{7} \sum_{j=0}^{7} \sum_{l=0}^{7} a_{ijl} g_i(R_{HO}) h_j(R_{OCl}) d_l(R_{ClH}), \quad (3)$$

with

$$g_i(R_{HO}) = [1 - e^{-k_{HO}(R_{HO} - \bar{R}_{HO})}]^i, \quad (4)$$

$$h_j(R_{OCl}) = [1 - e^{-k_{OCl}(R_{OCl} - \bar{R}_{OCl})}]^{j+1} - 1, \quad (5)$$

$$d_l(R_{ClH}) = [1 - e^{-k_{ClH}(R_{ClH} - \bar{R}_{ClH})}]^l. \quad (6)$$

The nonlinear parameters are: $\bar{R}_{HO} = 1.85 a_0$, $\bar{R}_{OCl} = 3.2 a_0$, $\bar{R}_{ClH} = 4 a_0$, $k_{HO} = 0.3 a_0^{-1}$, $k_{OCl} = 0.8 a_0^{-1}$, and $k_{ClH} = 0.1 a_0^{-1}$. All functions $h_j(R_{OCl})$ go to zero as R_{OCl} goes to infinity. In order to avoid spurious features at large distances, where fewer points have been calculated, the additional damping factor in Eq. (3) is introduced.

The linear parameters a_{ijl} are determined using a least-squares procedure employing a singular value decomposition.[47] In order to decrease the overall deviations from the *ab initio* points, we actually performed two independent fits; the resulting interaction potentials are denoted by $V_I^{(1)}$ and $V_I^{(2)}$, respectively. In the first fit, all points with energies below the HO+Cl threshold are taken into account with weight one, whereas points with energies above the threshold are given a smaller weight. In the second fit all points are included with identical weight. Thus, $V_I^{(1)}$ provides a more accurate description of the potential well, while $V_I^{(2)}$ gives a better description of the global potential, including both the well region and the repulsive parts of the potential. The final expression for the PES is a weighted sum of both fits, with a switching function which ensures that the two expressions are smoothly joined, i.e.,

$$V = (t - 1)V_I^{(1)} + t V_I^{(2)} + v_{HO}. \quad (7)$$

The switching function is defined by

$$t = \tfrac{1}{2}\{1 + \tanh[8(V_I^{(2)} + v_{HO} + 0.8)]\}. \quad (8)$$

The potential energies in Eq. (8) are given in electron volts. For energies below -0.8 eV the potential is mainly determined by $V_I^{(1)}$, whereas for energies above -0.8 eV, $V_I^{(2)}$ is the dominant part.

The rms deviation of the fit from the *ab initio* points is 5.9 meV including only points from the minimum to $E = 0$ and 8.8 meV, if points up to an energy of 4 eV above the threshold are taken into account. The deviations for points in

TABLE I. Equilibrium geometries (Å and deg.), dissociation energies (cm^{-1}), and fundamental transition frequencies (cm^{-1}).

	Original PES	Scaled PES	Experiment
R_{HO}^e	0.964	0.967	0.9644[a]
R_{OCl}^e	1.694	1.702	1.6890[a]
α^e	102.2	102.2	102.96[a]
D_e(HO-Cl)	20 366.6	20 366.6	—
D_0(HO-Cl)	19 347.3	19 349.9	19 290.3[b]
ν_1	3618.3	3602.2	3609.48[c]
ν_2	1245.9	1238.3	1238.62[d]
ν_3	726.0	724.6	724.36[d]

[a]The experimental equilibrium structure was taken from Refs. 48 and 49.
[b]Reference 28.
[c]Reference 50.
[d]Reference 51.

the vicinity of the equilibrium configuration are well below 1 meV. The sets of 2×512 linear parameters $a_{ijl}^{(1)}$ and $a_{ijl}^{(2)}$ as well as a FORTRAN code can be obtained from one of the authors (R.S.).

The calculated equilibrium structure agrees favorably with the experimental one (Table I). The dissociation energy D_0(HO–Cl) is also in good agreement with the experimental value. Including spin–orbit coupling in the calculations would decrease the dissociation energy and thereby further improve the calculated value. The deviations in the fundamental transition frequencies are 9, 7, and 2 cm^{-1} for modes 1, 2, and 3, respectively; (ν_1, ν_2, and ν_3 are the HO stretching, the bending, and the OCl stretching mode, respectively.) One of the goals of our study of HOCl is the decay of the overtone states (6,0,0) and (7,0,0), for which experimental results are available.[26–28] Although a deviation of only 9 cm^{-1} for the HO fundamental frequency is very satisfactory, the deviations for the higher overtones seem to be unacceptable. In order to further improve the agreement, we slightly scaled the two bond distances, i.e., $x \to \epsilon x$ with $\epsilon = 0.996$ for the HO bond and 0.998 for the OCl bond distance. While the original PES *overestimates* the HO stretching frequency by 9

TABLE II. Comparison of calculated and observed vibrational band origins (cm^{-1}).

(v_1, v_2, v_3)	Theory	Experiment	Expt'l. Ref.
0 0 0	0	0	
0 0 1	724.6	724.36	51
0 1 0	1238.3	1238.62	51
0 2 0	2458.2	2461.21	52
1 0 0	3602.2	3609.48	50
1 0 1	4323.8	4331.91	53
1 1 0	4813.8	4820.43	53
1 2 0	6003.3	6013.83	53
2 0 0	7036.7	7049.81	54
3 0 0	10 307.7	10 322.29	53
3 1 0	11 463.2	11 478.01	55
3 2 0	12 593.2	12 612.55	24
4 0 0	13 416.9	13 427.39	56
4 1 0	14 535.4	14 555.60	56
5 0 0	16 359.1	16 364.75	56
6 0 0	19 125.4	19 122.80	Cited in Ref. 29
7 0 0	21 715.6	21 709.07	27

cm^{-1}, the scaled PES *underestimates* it by 7 cm^{-1}. How-
ever, the scaling factor is chosen so that the disagreement
with the experimental energies is small for *all* states of the
$(v_1,0,0)$ progression with $v_1=1$ through 7 (see Table II).
The other two transition frequencies obtained with the scaled
PES are in very good agreement with experiment. The scal-
ing slightly modifies also the equilibrium bond distances.
This could be corrected for by a tiny translation of the two
stretch coordinates, which, however, has not been done. All
dynamics calculations, which will be presented in the follow-
ing, are performed with the scaled PES.

In Table II we compare vibrational band origins with
available experimental data. The agreement is satisfactory
with the largest deviation being 20 cm^{-1} and a rms deviation
of 11 cm^{-1}.

There are two other PESs available for HOCl, which
have been constructed very recently. Peterson[57] determined a
near-equilibrium PES based on high quality coupled cluster
ab initio calculations. With this PES the experimentally
known overtones and combination bands up to energies of
about 10 000 cm^{-1} were accurately reproduced. However,
because this PES is restricted to configurations not too far
from equilibrium, it cannot be used for studying the frag-
mentation into HO and Cl. Similar *ab initio* calculations on
an even higher level of accuracy were subsequently per-
formed by Koput and Peterson.[58] Skokov, Peterson, and
Bowman[29] extended the calculations of Peterson and con-
structed a global PES, which is suited to study high over-
tones of the HO stretching mode as well as dissociation into
HO+Cl. The *ab initio* level is comparable to the level of
accuracy used in our calculations. Skokov, Peterson, and
Bowman, however, performed a more elaborate scaling pro-
cedure and therefore their PES reproduces the experimen-
tally known vibrational energies slightly better than our sur-
face. The general topographies of the two potential surfaces
are very similar.

Figure 1 depicts three two-dimensional cuts through the
PES. The coordinates are the Jacobi coordinates appropriate
for dissociation into HO and Cl: R, the distance from Cl to
the center of mass of HO, r, the HO bond distance, and γ,
the angle between the two vectors $\mathbf{R}$ and $\mathbf{r}$ ($\gamma=180°$ corre-
sponds to linear HOCl). The two dissociation channels,
HO+Cl ($R\rightarrow\infty$) and H+OCl ($r\rightarrow\infty$), are clearly seen in
Fig. 1 (middle panel). However, the latter one is consider-
ably higher in energy and therefore is of no consequence for
our study. There is no barrier in the HO+Cl exit channel
(Fig. 2). In the linear geometry, $\gamma=180°$, two pronounced
maxima exist, which are caused by conical intersections with
higher electronic states.[29] The first one occurs near $R\approx4a_0$
[Fig. 1 (upper panel)] and the second one is located at large
HO distances [Fig. 1 (lower panel)].

The main characteristic of the HOCl ground-state PES is
the weak potential coupling between the three internal de-
grees of freedom. The minimum energy paths are almost
perfectly aligned along the respective coordinate axes. At
low energies the same is true for the nodal lines of the quan-
tum mechanical wave functions. At higher energies, how-
ever, an anharmonic resonance between R and γ is devel-
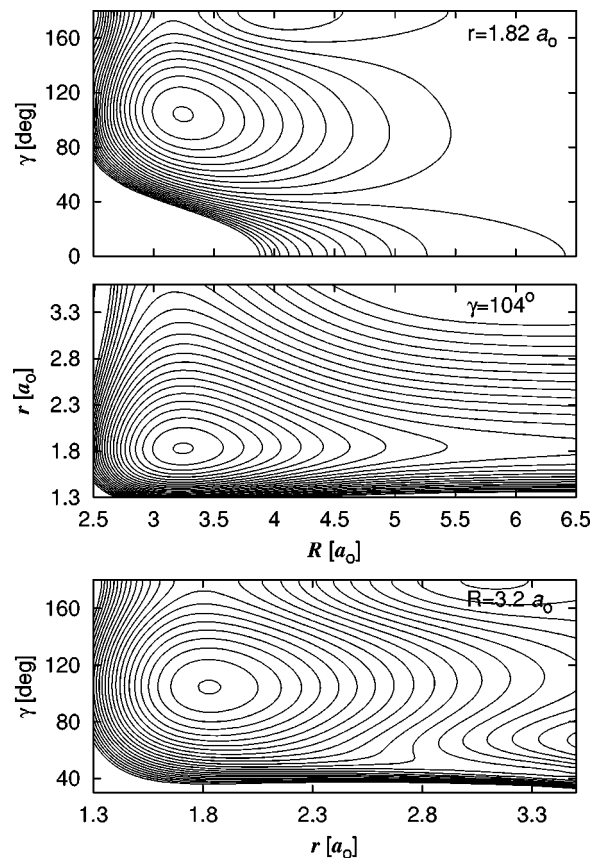oped, which strongly changes this simple picture.

FIG. 1. Contour plots of the HOCl ground-state PES. The contour spacing is
0.25 eV and the highest energy in each panel is 3 eV. Energy normalization
is such that $E=0$ corresponds to HO+Cl with HO at equilibrium.

III. CALCULATION OF BOUND AND RESONANCE STATES

All dynamics calculations are performed using the filter
diagonalization method.[59–61] In a first step, optimally
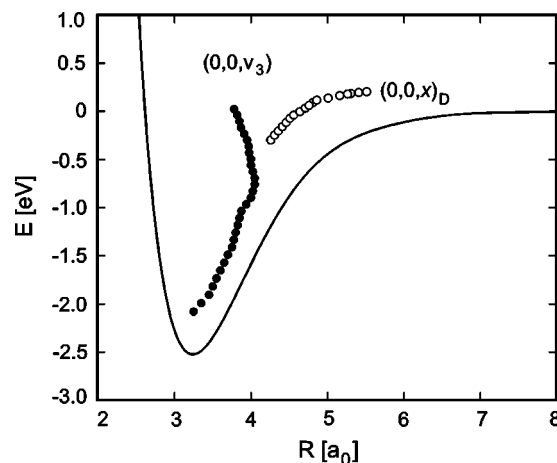adapted basis functions (so-called 'window basis functions')

FIG. 2. Minimum energy path along the dissociation coordinate R; the po-
tential is minimized in the other two degrees of freedom. The symbols
indicate the extension of wave functions in the two progressions $(0,0,v_3)$
and $(0,0,x)_D$, respectively (see the text).

Ψ_i, which span only a relatively small subspace of the whole Hilbert space, are generated by applying the Green's function

$$\hat{G}^+(E_i)=(E_i-\hat{H}+iW)^{-1} \tag{9}$$

as a filtering operator onto an initial wave packet χ,

$$\Psi_i=\operatorname{Im}\hat{G}^+(E_i)\chi, \tag{10}$$

where iW is a complex absorbing potential ($W=0$ for bound-states calculations). The energies E_i are taken to be equally spaced in the interval $[E_{min},E_{max}]$. The filtering is efficiently performed using the (modified) Chebychev polynomial expansion of the Green's function.[60–64] In the second step the eigenstates in the energy window $[E_{min},E_{max}]$ are calculated by diagonalizing the Hamiltonian in the small set of basis functions Ψ_i.

Because the window basis functions are explicitly stored in the core memory of the computer, it is necessary to carefully choose the size of the energy windows $[E_{min},E_{max}]$. As a rule of thumb, the number of basis functions for a particular interval should be roughly twice the number of eigenstates as estimated from the expected density of states in this window. In the present case we have calculated all the 827 bound states supported by our PES in 13 overlapping energy windows, where we tried to keep the number of eigenstates per window roughly constant. While the lowest energy window ranged from -2.2 to -1.3 eV, the highest window covered an energy region of only 0.03 eV. None of the calculations needed more than 300 Mbytes of main memory.

For the highest lying energy window the three-dimensional grid was chosen to extend from $2.5a_0$ to $10.0a_0$ in R with 150 potential-optimized points,[65] from $1.0a_0$ to $3.5a_0$ in r with 30 potential-optimized points, and from $0°$ to $180°$ in the angular coordinate with 70 Gauss–Legendre quadrature points.[66] The grid size of $N=315\,000$ points has been further reduced to $N=197\,000$ points by discarding all points with potential energies larger than 1.8 eV. We found that 60 000 Chebychev iterations were sufficient for converging even the highest bound states of HOCl.

The calculation of the complex resonance energies above the HO+Cl dissociation threshold has been performed by adding an imaginary (absorbing) potential[67–69] iW to the Hamiltonian [see Eq. (9)].[60,61,63,64] It enters the filtering procedure in the form of a damping operator $\exp[-\hat{\gamma}(R)]$. Following Mandelshtam and Taylor, the coordinate dependent function $\hat{\gamma}(R)$ is assumed to have the form[60,61,63]

$$\hat{\gamma}(R)=\frac{D_0}{(\Delta H)^{1/2}}\left(\frac{R-R_{damp}}{R_{max}-R_{damp}}\right)^2\Theta(R-R_{damp}). \tag{11}$$

Here, ΔH (in atomic units) and Θ denote the spectral range of the Hamiltonian and the Heaviside step function, respectively. The three adjustable parameters are the damping strength, D_0, the starting point for the absorbing potential, R_{damp}, and the end point of the grid in the dissociation coordinate, R_{max}. The relationship between $\hat{\gamma}$ and W is explicitly given in Ref. 64. After many test calculations we found the following parameters to give tolerable resonance widths: $R_{max}=14a_0$, $R_{damp}=12a_0$, and $D_0=0.1$. Because the grid is

significantly extended in the R direction as compared to the bound-states calculations, the number of grid points in the dissociation coordinate is increased to 220. In addition, we observed that an unexpectedly high number of Chebychev iterations (180 000) is required for converging the resonance widths of states having substantial excitation in the HO stretching mode.

IV. CHARACTERIZATION OF BOUND STATES

We have calculated all the bound states up to the HO+Cl dissociation threshold—827 on our PES—and we have visually inspected each of them in order to recognize how the structure of the spectrum changes with energy. [A list of all bound state energies and assignments is available electronically[70] or can be obtained from one of the authors (R.S.).] The inspection ''by eye'' is indispensable, we believe, for making the correct assignment. The energy level spectrum of HOCl is simple and the assignment of the vibrational states is straightforward up to about four-fifths of the dissociation limit. Then, however, complications related to a saddle-node bifurcation of the corresponding classical phase space occur, which make the interpretation considerably more complicated. We will first discuss the low-energy regime and subsequently focus on the changes happening at higher energies. The coupling between the HO stretching mode and the other two degrees of freedom is very weak, so that it is justified to analyze the manifolds for different values of v_1 separately.

A. Polyad structure for $v_1=0$ in the low-energy regime

At low energies all states can be clearly assigned in terms of quantum numbers (v_1,v_2,v_3). The wave functions of the pure overtone states $(v_1,0,0)$, $(0,v_2,0)$, and $(0,0,v_3)$ are basically aligned along the HO stretch coordinate r, the angular coordinate γ, and the dissociation coordinate R, respectively. The fundamental OCl frequency is slightly larger than half of the fundamental bending frequency, that is, the spectrum is governed by an approximate 1:2 anharmonic resonance: Two quanta of OCl stretch are roughly worth one quantum of the bending mode. As a consequence, the spectrum is organized, for a given HO quantum number v_1, in polyads denoted by $[\![v_1,P]\!]$. The polyad quantum number is defined by $P=2v_2+v_3$. Figure 3 illustrates the polyad structure of the energy levels for $v_1=0$ in the range of polyads $[\![0,19]\!]$ through $[\![0,30]\!]$. The spectra with excitation of the HO stretching coordinate are virtually replicas of the $v_1=0$ spectrum, roughly shifted by one, two, etc., HO vibrational quanta to higher energies (see the following). The number of states in each polyad is $(P+2)/2$ for even values of P and $(P+1)/2$ for odd polyad quantum numbers. Already at low energies the polyads significantly overlap. The OCl stretching states $(0,0,P)$ are always at the top of each polyad, whereas — up to polyad $[\![0,27]\!]$ — the bending overtones $(0,v_2,0)$ or $(0,v_2,1)$ demarcate the lower end. Around the energy of -0.5 eV structural changes occur, which are discussed in detail in Sec. IV B.

In order to illustrate the general behavior of wave functions in the low-energy regime, we depict in Fig. 4 the wave
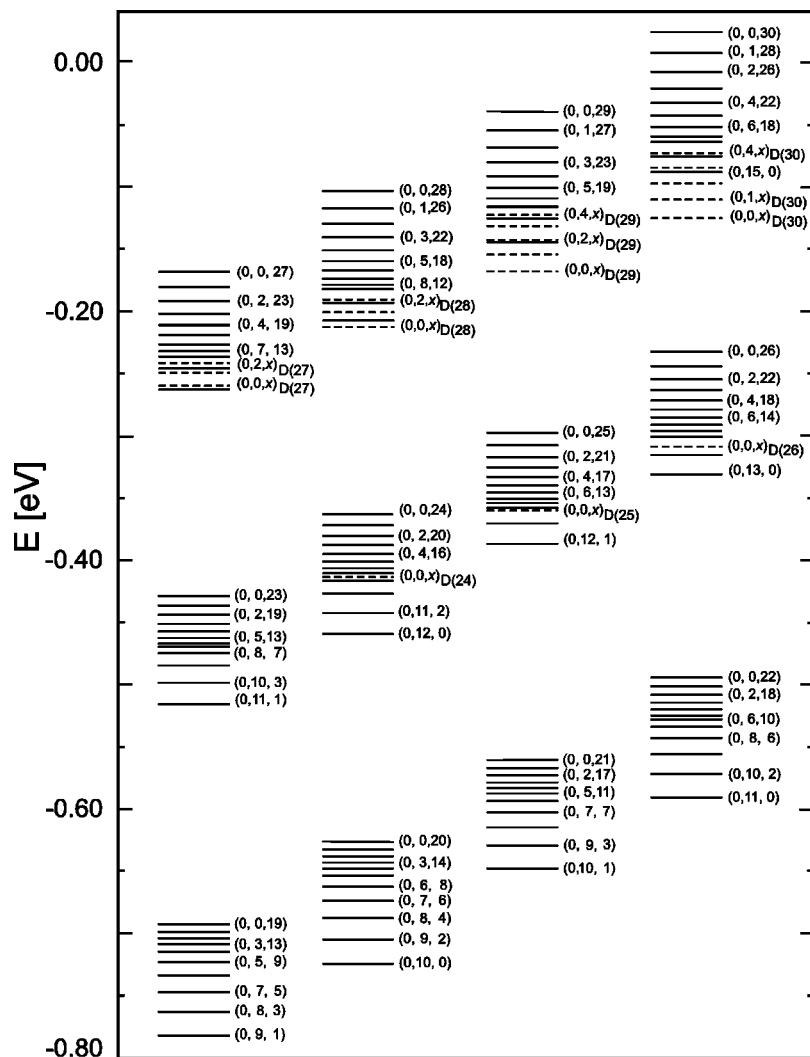
E [eV]

0.00

−0.20

−0.40

−0.60

−0.80

(0, 0,30)
(0, 1,28)
(0, 2,26)
(0, 4,22)
(0, 6,18)
$(0,4,x)_{D(30)}$
(0,15, 0)
$(0,1,x)_{D(30)}$
$(0,0,x)_{D(30)}$

(0, 0,29)
(0, 1,27)
(0, 3,23)
(0, 5,19)
$(0,4,x)_{D(29)}$
$(0,2,x)_{D(29)}$
$(0,0,x)_{D(29)}$

(0, 0,28)
(0, 1,26)
(0, 3,22)
(0, 5,18)
(0, 8,12)
$(0,2,x)_{D(28)}$
$(0,0,x)_{D(28)}$

(0, 0, 27)
(0, 2, 23)
(0, 4, 19)
(0, 7, 13)
$(0,2,x)_{D(27)}$
$(0,0,x)_{D(27)}$

(0, 0,26)
(0, 2,22)
(0, 4,18)
(0, 6,14)
$(0,0,x)_{D(26)}$
(0,13, 0)

(0, 0,25)
(0, 2,21)
(0, 4,17)
(0, 6,13)
$(0,0,x)_{D(25)}$
(0,12, 1)

(0, 0,24)
(0, 2,20)
(0, 4,16)
$(0,0,x)_{D(24)}$

(0, 0,23)
(0, 2,19)
(0, 5,13)
(0, 8, 7)
(0,10, 3)
(0,11, 1)

(0,11, 2)
(0,12, 0)

(0, 0,22)
(0, 2,18)
(0, 6,10)
(0, 8, 6)
(0,10, 2)
(0,11, 0)

(0, 0,21)
(0, 2,17)
(0, 5,11)
(0, 7, 7)

(0, 9, 3)
(0,10, 1)

(0, 0,20)
(0, 3,14)
(0, 6, 8)
(0, 7, 6)
(0, 8, 4)
(0, 9, 2)
(0,10, 0)

(0, 0,19)
(0, 3,13)
(0, 5, 9)
(0, 7, 5)
(0, 8, 3)
(0, 9, 1)

FIG. 3. Energy level spectrum in the region of polyads $[\![0,19]\!]$–$[\![0,30]\!]$. The dissociation states $(0,v_2,x)_{D(P)}$ are indicated by dashed lines.

functions for all states of the $[\![0,12]\!]$ polyad. We plot them in the (R,γ) plane because of the resonance between the bending and the OCl stretching degrees of freedom. The labeling with quantum numbers is straightforward: They specify the number of nodes along the three coordinate axes. Because of the relatively large mismatch of more than 100 cm^{-1} between $\nu_2/2$ and ν_3, the mixing between R and γ is not well developed in the lower energy region and the wave functions do not show the general structure characteristic for a 1:2 resonance.[8,71] The backbones of the wave functions for states $(0,P/2,0)$ and $(0,0,P)$ are almost perpendicular to each other.

However, being the dissociation mode, the OCl stretch is much more anharmonic than the bend. Therefore, the mismatch between the corresponding transition frequencies gradually decreases and the resonance condition becomes better and better fulfilled, as it is seen in Fig. 5(c), where we show for the two progressions $(0,0,P)$ and $(0,P/2,0)$ the energy gap between adjacent levels as functions of energy. The transition frequencies of the bending mode are divided by two. The two frequency curves come very close to each other near $P \approx 16$ and remain close until $P \approx 25$. The more and more exact resonance leads to an increasing mixing between the R and the γ motions, at least for the states at the

upper ends of the polyads. For example, the $(0,0,P)$ wave functions become gradually more curved in the (R,γ) plane as illustrated in the left-hand panel of Fig. 6. The curvature is already present for polyad $P=12$ (Fig. 4), but it becomes clearly pronounced not until P is larger than 16 or so. This horseshoe-type behavior is typical for systems governed by a 1:2 resonance.[8] As a consequence of the mixing, the states which at low energies start out to advance along the dissociation coordinate, R_{OCl}, at high energies avoid the dissociation path. This is illustrated in Fig. 2, where we plot the value of the dissociation coordinate, R_{max}, at which the $(0,0,P)$ wave functions have their outermost maximum, versus energy. R_{max} first increases with P, reaches a maximum around $P \approx 17$–18, and then again decreases slightly. As will be discussed in Sec. V, the backbones of the $(0,0,P)$ wave functions are scarred by a stable classical periodic orbit (PO). Because of the strong mixing, referring to the $(0,0,P)$ states as ''OCl stretching states'' is meaningless, except in the low-energy regime. The quantum number v_3 denotes the number of nodes along the corresponding PO, rather than along the R axis. In contrast, the wave functions of the states at the bottom of the polyads, $(0,P/2,0)$, retain their general shape from low to very high energies. They do not show the behavior representative for a 1:2 resonance. Their backbones
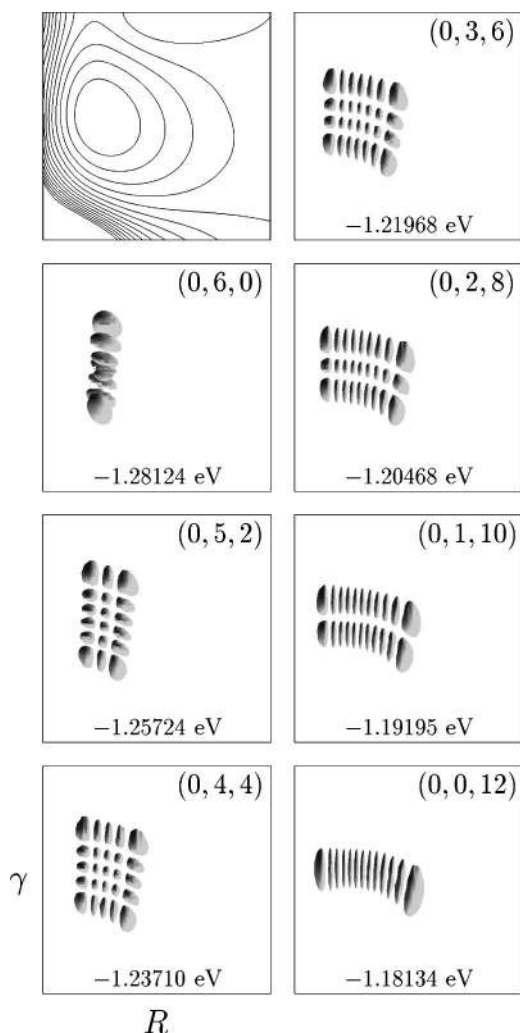
J. Chem. Phys., Vol. 112, No. 1, 1 January 2000

Bifurcations in the spectrum of HOCl   83

FIG. 4. Wave functions for polyad $P = 12$. The γ axis ranges from 19° to 179° and the R axis ranges from $2.5a_0$ to $5.42a_0$. All wave function plots depicted in this article, if not stated otherwise, have been obtained from a plotting routine which allows one to rotate 3D objects in space. Shown is one particular contour $\epsilon(R, r, \gamma) = |\Psi(R, r, \gamma)|^2$ with the value of ϵ being the same in each figure. The plots are viewed along one coordinate axis, in the direction perpendicular to the plane of the other two coordinates. Shading emphasizes the 3D character of the wave functions. The potential is shown in the upper left-hand panel. The numbers are the energies of the respective quantum states.
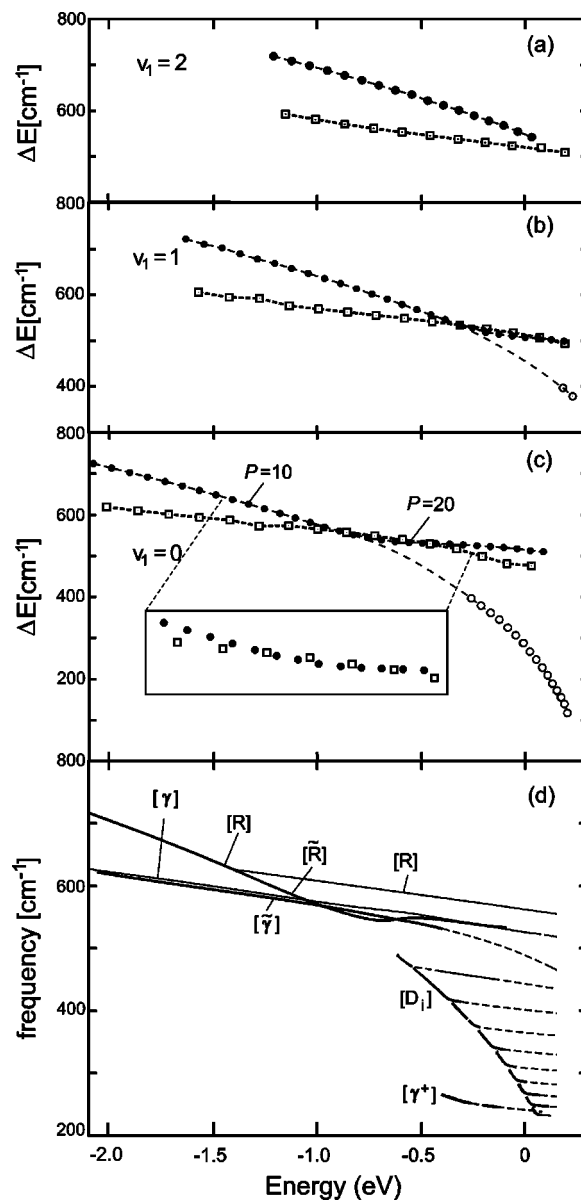

FIG. 5. (a)–(c) Energy difference between adjacent states of the pure progressions $(v_1, 0, v_3)$, $(v_1, v_2, 0)$, and $(v_1, 0, x)_{D(P)}$ as function of energy for $v_1 = 0, 1$, and 2. The inset in (c) shows an enlargement of the "crossing region." (d) Frequencies of the classical periodic orbits belonging to various families. Solid lines indicate stable POs and dashed lines represent unstable ones. The branches, which influence the quantum mechanical states, are indicated by the thicker solid lines. The frequencies of the $(0, v_2, 0)$ states and, likewise, the frequencies of the $[\gamma]$-, $[\tilde{\gamma}]$-, and $[\gamma^+]$-type POs are divided by two. See the text for more details.

are also scarred by a stable PO (see the following).

A quantity, which to some extent reflects the degree of mixing, is the energy spacing between adjacent levels inside the polyads. In Fig. 7 we depict $\Delta E = E_n^P - E_{n-1}^P$ as function of n for various polyads P; the index n specifies the state inside the polyad with $n = 0$ being the lowest state. In the low-P region, ΔE is a smooth, monotonically decreasing function with its minimum value at the top of the polyad. Between $P = 16$ and 18, however, the energy spacing curve loses its monotonic behavior.

B. Genesis of dissociation states

The increasing coupling between R and γ with increasing energy and the resulting mixing leads — above polyad $[\![0,21]\!]$ — to a gradual distortion of the simple appearances of the wave functions observed for the lower polyads. This dis-

tortion is most pronounced for the states in the middle of the polyads, whereas the states near the bottom or the top of a polyad still can be characterized and assigned in the same manner as for the lower polyads. Figure 8 illustrates these changes in the wave function character for selected states belonging to polyads $[\![0,21]\!]$ through $[\![0,25]\!]$. The way in which the assignment is done, i.e., the "axes" along which the number of nodes v_2 and v_3 are counted, is illustrated by the arrows in some of the panels.

The wave function for state $(0,7,8)$ in polyad $[\![0,22]\!]$ still has a structure, which matches the behavior of the wave functions in the lower polyads and its assignment is quite
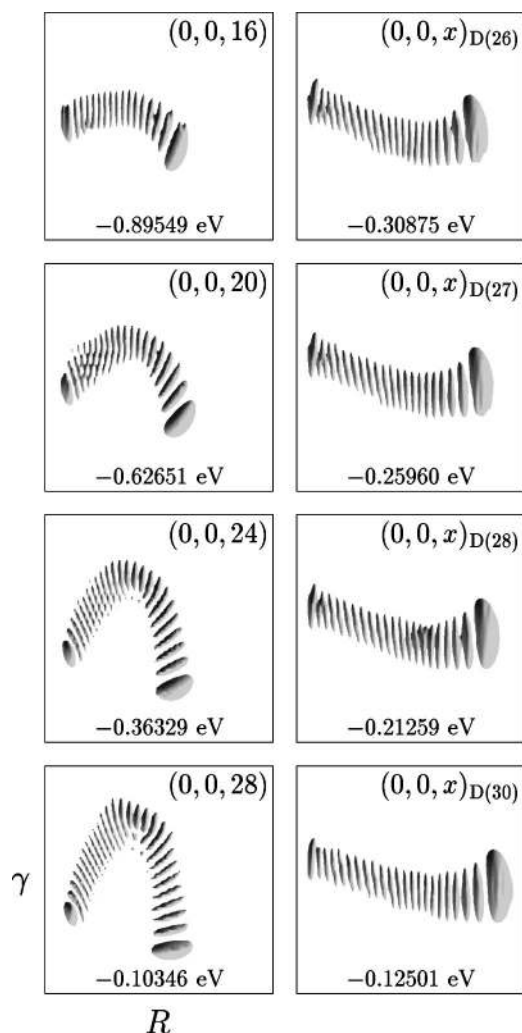
FIG. 6. Wave functions of the pure overtone states $(0,0,P)$ (left-hand column) and the dissociation states $(0,0,x)_{D(P)}$ (right-hand column). For further details see Fig. 4.

FIG. 7. Energy spacings between neighboring states inside the polyads $[\![0,14]\!]$–$[\![0,28]\!]$ as function of n, where n indicates the position in the polyad ($n=0$ for the lowest state).

clear. The appearance of the wave functions for the next three higher states, however, is more involved, especially for state $(0,6,10)$. Making the same plot with a lower contour level shows a slightly different nodal structure and in particular reveals that the assignment as $(0,6,10)$ can still be justified. Nevertheless, the general appearance of the $(0,6,10)$ wave function is different from that for state $(0,7,8)$: There is a central "backbone" along which the amplitude is maximal. Such a backbone is missing for $(0,7,8)$. The wave functions for the higher states in this polyad, $(0,5,12)$, $(0,4,14)$, etc., have shapes, which resemble the nodal structures known from the states in the lower polyads.

The particular shape of the $(0,6,10)$ wave function becomes more evident in the higher polyads: See, e.g., the wave functions for state $(0,7,9)$ for $P=23$, $(0,8,8)$ for $P=24$, and $(0,9,7)$ for $P=25$. While the wave functions for states $(0,6,10)$ and $(0,7,9)$ still show amplitude off the main backbone, the wave functions for states $(0,8,8)$ and $(0,9,7)$ are much more distinct, i.e., the amplitude outside the region of the backbone is marginally small.

The assignment of the fifth ($n=4$) state in polyad $P=23$ as $(0,7,9)$ is nonetheless justified: Plotting the wave
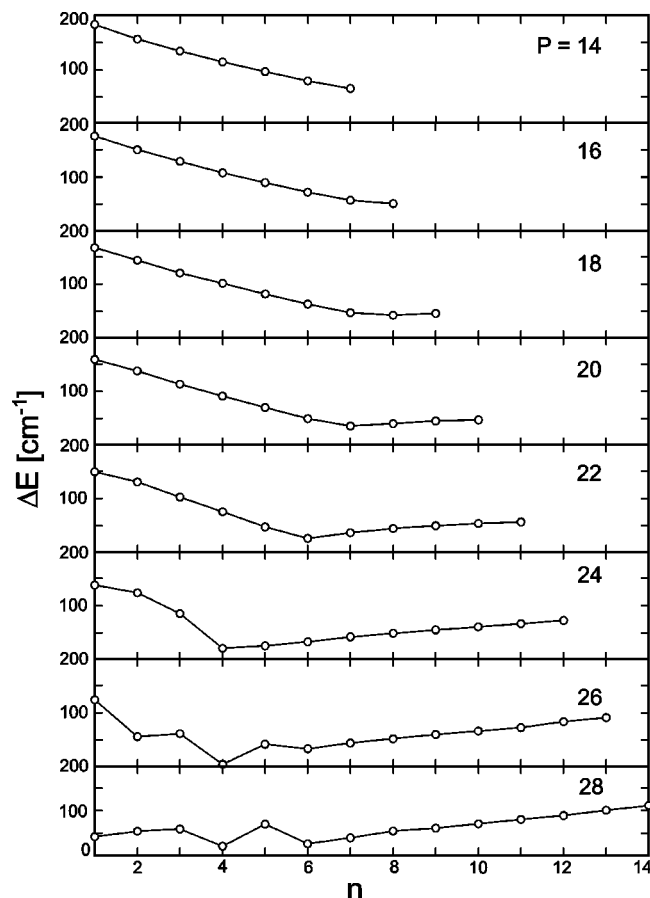
function at a lower contour level reveals that it has 7 and 9 nodes, respectively, along the v_2 and v_3 "axes," which are indicated in Fig. 8. On the other hand, the assignments of the $n=4$ state of $P=24$ and the $n=2$ state in polyad $P=25$ as $(0,8,8)$ and $(0,9,7)$, respectively, are not at all reasonable. The labels $(0,8,8)$ and $(0,9,7)$ merely indicate that at these positions states with these assignments are expected. However, such states are missing and their positions are occupied by these new states. In order to distinguish the "new" states from the "normal" ones, we will assign them as $(v_1,v_2,x)_{D(P)}$, where the abbreviation D stands for "dissociation" and the number in parentheses indicates the polyad this state belongs to. With increasing polyad quantum number combination states of the D type with one, two, and more nodes in the direction perpendicular to the main backbone, i.e., with excitation essentially in the bending mode, come into existence, e.g., state $(0,8,9)$ for polyad $P=25$.

The number of nodes along the backbones of these functions is not identical to the polyad quantum number P. For example, the $(0,0,x)_{D(24)}$ wave function for polyad $P=24$ has only 19 nodes. (It, beyond any doubt, is not a member of polyad $P=19$.) Because of the mismatch between the polyad quantum number P and the actual number of nodes along the backbone, we replace the quantum number v_3 by x without specifying the value of x. As before, v_1 is the number of HO stretching quanta and v_2 refers to the number of quanta in
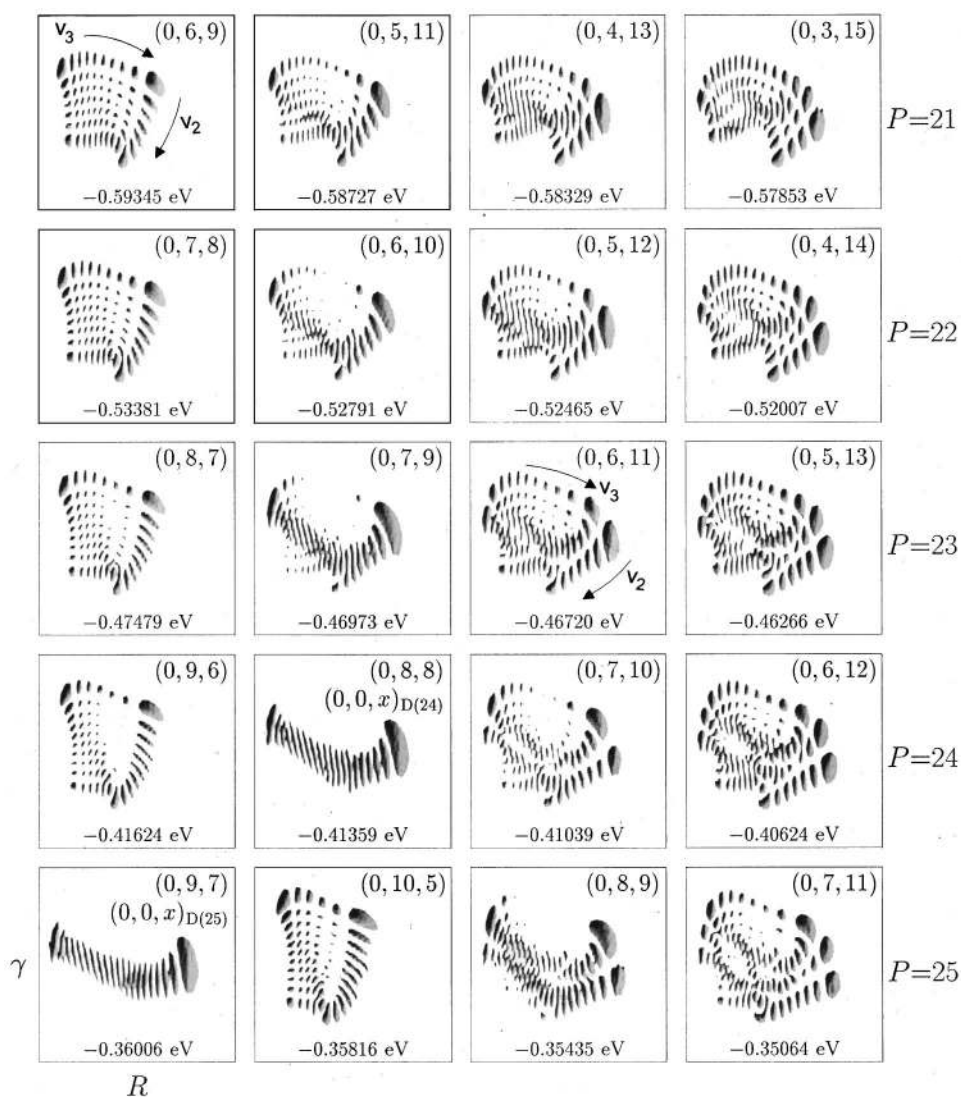
FIG. 8. Selected wave functions for polyads $[\![0,21]\!]$–$[\![0,25]\!]$ illustrating the gradual distortion of the nodal behavior observed for the lower polyads and the genesis of the $(v_1,v_2,x)_{D(P)}$ dissociation states. For further details see Fig. 4.

the direction perpendicular to the backbone, basically the angular coordinate. There is another peculiarity. The number of nodes of the D states along their backbones does not necessarily increase by one when going from one polyad to the next higher one. For example, the wave functions for states $(0,0,x)_{D(24)}$ and $(0,0,x)_{D(25)}$ both have 19 nodes. Moreover, it is possible that the number of nodes along the backbones is identical for states $(0,0,x)_{D(P)}$ and $(0,1,x)_{D(P)}$. The allocation to a particular polyad is only possible by carefully following how the spectrum and the wave functions develop from low energies to high energies and this requires one to inspect each wave function state by state.

The D states clearly follow the dissociation path, i.e., they extend further and further into the HO+Cl fragment channel when the energy increases (Fig. 2 and the right-hand panel of Fig. 6). They form a new family of states, which does not exist at lower energies, but comes into existence abruptly at high energies. As we will show in Sec. V, the D states can be interpreted as the consequence of a saddle-node bifurcation of the classical phase space. Details of the quantum mechanical/classical correspondence will become clearer in the two-dimensional study.[33] The birth of the D

states leaves the number of states per polyad intact; it is the structure of the individual polyads, i.e., the wave functions and the energy spacings between neighboring states (see the following), that is considerably changed by the D states. The alterations become rapidly more severe with increasing energy.

The evolution of the wave functions as illustrated in Fig. 8 continues at higher polyads, namely some of the ''normal'' states, which are well assignable in the lower polyads, disappear and at the same time new D states are born. Since the D states advance along the dissociation path, they show a considerable anharmonicity as indicated by the energy level spacing between adjacent $(0,0,x)_{D(P)}$ states in Fig. 5(c). The curve of transition frequencies for the D states seems to be the continuation of the curve for the $(0,0,v_3)$ states, i.e., the states which in the low energy regime have mainly OCl stretching character. The extrapolation of the $(0,0,x)_{D(P)}$ curve to lower energies merges with the $(0,0,v_3)$ frequency curve around $P \approx 16$–17 ($E \approx -0.9$ eV), just in the region where the frequency curves for the states $(0,0,v_3)$ and $(0,v_2,0)$ intersect each other, i.e., where the two transition frequencies are almost identical.
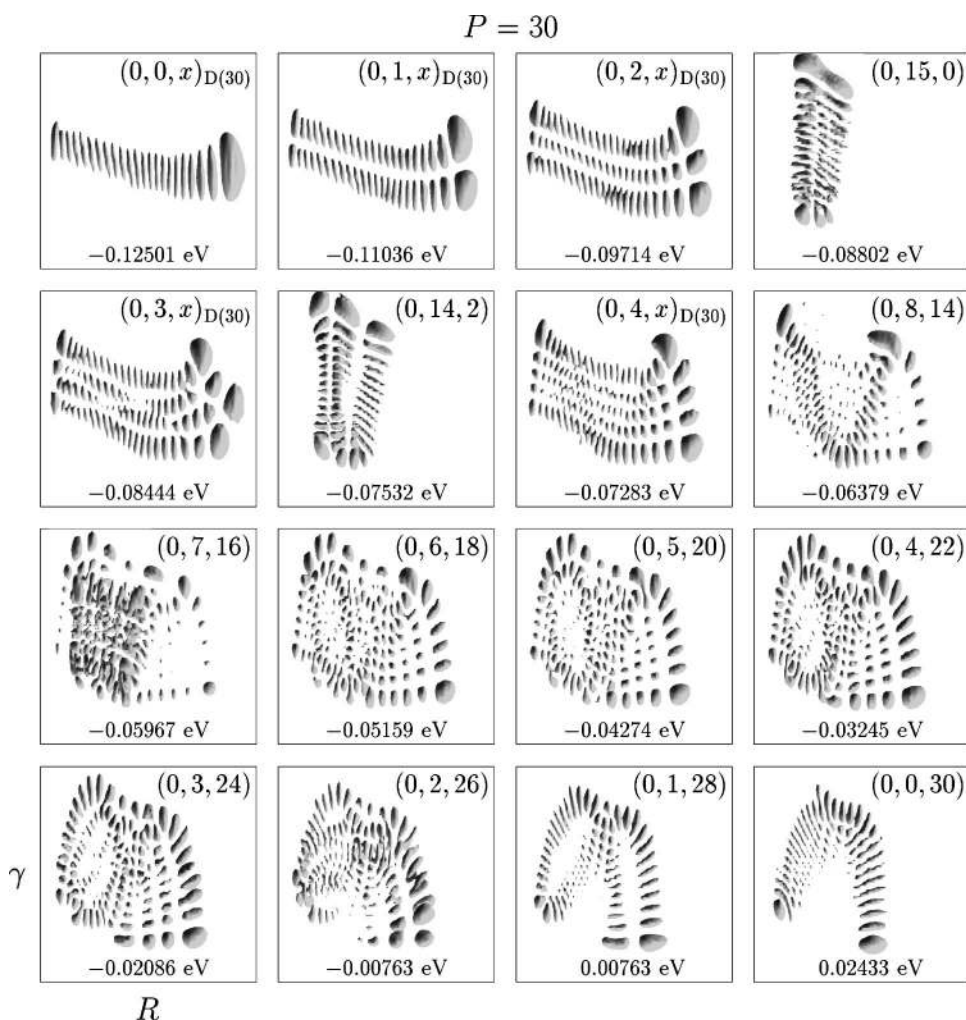
$$P = 30$$

FIG. 9. All wave functions for polyad $[\![0,30]\!]$. For further details see Fig. 4.

The energy-level spectrum of HOCl becomes quite complex in the high-polyad regime. When the D states come into existence around $P = 23$–24, they are born in the middle of the respective polyads. However, because of the large anharmonicity, they quickly move to the lower ends (Fig. 3). In polyad $[\![0,28]\!]$ it happens for the first time that an $(0,0,x)_{D(P)}$ state is the lowest state in a polyad. From there on, more and more states with D character and several quanta in the bending mode appear at the lower parts of the polyads. That the upper end of a polyad overlaps with the lower part of the next higher polyad does happen even at low energies, where D states do not yet exist. However, in the high-P regime it occurs that several polyads overlap. For example, the upper part of polyad $P = 28$ overlaps with states from polyads 29 and 30. This makes the analysis of the energy level spectrum cumbersome, especially if the wave functions are not available.

The problems related to the assignment rapidly grow as one approaches the dissociation limit. Actually, polyad $[\![0,31]\!]$ is the last one for $v_1 = 0$ that can be completely assigned. The number of unassignable states quickly gets larger for energies $E > 0$. In order to demonstrate the complexity of the wave functions at high energies we show in Fig. 9 all wave functions for polyad $[\![0,30]\!]$. The three lowest states are clear-cut D states of the form $(0,v_2,x)_{D(30)}$. They

are followed by a region in which D states and bending states alternate. The states in the middle of the polyad have an extremely complex nodal structure, whereas the top of the polyad again is governed by levels, which have the same general behavior as observed in the lower polyads and the assignment is rather clear. The highest state, $(0,0,30)$, has mainly bending character, although the lowest members of this progression started out to have excitation along the OCl stretching degree of freedom.

There is a further detail worth mentioning. The $(0,15,0)$ wave function has a clear node along the R coordinate, which is in contradiction to the general building principle of the polyads, i.e., the wave functions for the states $(0,v_2,0)$ have no node in the R direction. Again, this effect has a counterpart in the analysis of the classical phase space: At a period-doubling bifurcation of the bending family of POs the PO describing pure motion in γ becomes unstable and a new stable PO is created (see Sec. V). The latter one has the form of a very narrow horseshoe and it is this PO which scars the $(0,v_2,0)$ wave functions. The same effect also occurs in the 2D calculations and is even more clearly conceivable there.[33]

The emergence of the D states has a profound impact on the energy spacings inside the polyads (Fig. 7). While ΔE is a smooth and monotonically decreasing function in the low-P region, between $P = 16$ and 18 a very shallow mini-

mum develops in the top part of the polyads. With increasing polyad quantum number this minimum becomes more pronounced and gradually shifts toward the bottom of the polyad. The location of the minimum in the intrapolyad energy spacing is closely related to the $(0,0,x)_{D(P)}$ states. For example, for $P=22$ the minimum is at $n=6$ and the D state in this polyad is the sixth state; for $P=24$ the D state is the fifth state of this polyad and the minimum occurs at $n=4$. As P increases the D states rapidly move to the bottom part of the polyads and so does the minimum in the intrapolyad energy spacing. The ''fluctuations'' for the higher polyads, $P=26$ for example, are the consequence of the occurrence of more than one D state and their alternation with the ''normal'' states (Fig. 9).

The minimum begins to develop in polyads $P=16–18$. This is exactly the region in which the mixing between γ and R at the top of the polyads gets large because of the almost perfect degeneracy (see Fig. 5). As previously discussed, this is also the region in which the D states begin to come into existence. States with a clear-cut ''dissociation'' behavior do not show up before $P=21$. However, an extrapolation of the $(0,0,x)_{D(P)}$ frequency curve to lower polyads suggests that first indications already occur as early as $P\approx16–18$. In other words, the intrapolyad energy spacing is a very sensitive probe of the saddle-node bifurcation through which the D states are born. The relation between a minimum in the intrapolyad energy spacing and saddle-node bifurcations had been previously discussed by Svitac et al.[72] for a model resonance Hamiltonian and by Joyeux et al.[73] for HCP. It is interesting to note that well below the resonance region, ΔE is a monotonically decreasing function of n, while in the higher polyads, when the resonance behavior is fully developed, ΔE monotonically rises with n, except for the fluctuations at the bottom of the polyad. A detailed analysis is given in Ref. 33.

C. Polyad structure for $v_1 \geqslant 0$

Up to now we have only discussed the polyad structure for states in which the HO moiety is not excited, $v_1=0$. Because of the weak potential coupling between r on one hand and R and γ on the other, and because of the relatively large mismatch of the fundamental frequencies, $\nu_1/\nu_2 \approx \nu_1/2\nu_3 \approx 3$, the HO stretching motion is to a large degree separated from the motions in R and γ. As a consequence, the polyad structures for $v_1=1$ and 2 are almost replicas of the spectrum for $v_1=0$, merely shifted by the corresponding excitation energies. This general behavior is, for example, confirmed by the frequency curves for $v_1=1$ and 2 in Fig. 5. The point of intersection of the curves for the two progressions $(1,0,v_3)$ and $(1,v_2,0)$ is shifted by about 4600 cm^{-1} to higher energies with respect to the curves with $v_1=0$. As a result, the D states occur at energies very close to the dissociation threshold. The point of intersection is further shifted to higher energies for two quanta of excitation of the HO mode; D states with $v_1=2$ occur only in the continuum. The weak coupling between HO stretching motion and the other two degrees of freedom (together with the fact that ν_1
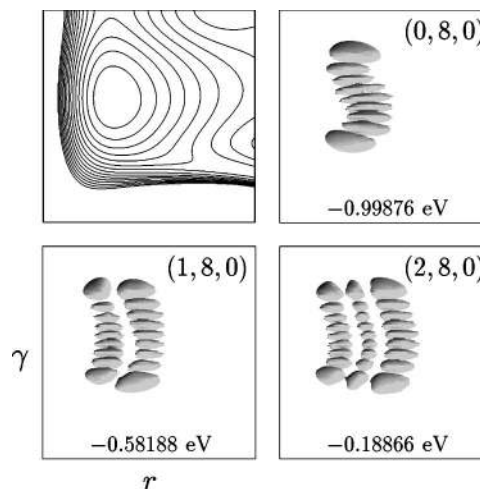

FIG. 10. Examples of $(v_1,v_2,0)$ wave functions in the (r,γ) plane. The γ axis ranges from 1° to 179° and the r axis ranges from $1.0a_0$ to $3.5a_0$.

$\gg \nu_{2,3}$) is responsible for the success of the two-dimensional model in reproducing — and explaining — the results of the present three-dimensional study.[33]

Although the coupling between r, on the one hand, and R and γ, on the other, is weak, it is not negligible. This can be seen in Fig. 10, where we depict the wave functions for states $(0,8,0)$, $(1,8,0)$, and $(2,8,0)$ in the (r,γ) plane. The wave function for state $(0,8,0)$ shows an undulatory behavior, which is characteristic for a 3:1 resonance system,[6] i.e., one quantum of HO stretch is worth three quanta of the bending mode. As will be discussed in the Sec. V, the precise shape of the $(0,v_2,0)$ wave functions in the (r,γ) plane is helpful in finding those periodic orbits which correspond to the quantum wave functions. The wave functions for the states with excitation in r show a different behavior; they are slightly bent without the characteristic 3:1 resonance behavior.

V. ANALYSIS OF THE CLASSICAL PHASE SPACE

The structure of the quantum mechanical spectrum and particularly the shapes of the wave functions can be elucidated in terms of the structure of the classical phase space and special trajectories therein, so-called periodic orbits (POs).[18,74] POs are classified as stable or unstable depending on the eigenvalues of the monodromy matrix.[15] For many systems it has been demonstrated that the ''backbones'' of quantum mechanical wave functions closely follow certain stable POs.[75] HOCl is a particularly illuminating system for illustrating the close correspondence between the phase-space structure and the quantum mechanical spectrum, all the way from the bottom of the potential well to the dissociation threshold.

Despite the remarkable simplicity of the quantum mechanical spectrum up to high energies, the structure of the classical phase space is quite involved already at low energies. Near the bottom of the well there are three types of POs, the principal families. They are denoted by $[r]$, $[\gamma]$, and $[R]$, respectively, because the POs basically describe motions along the three coordinate axes. Instead of showing
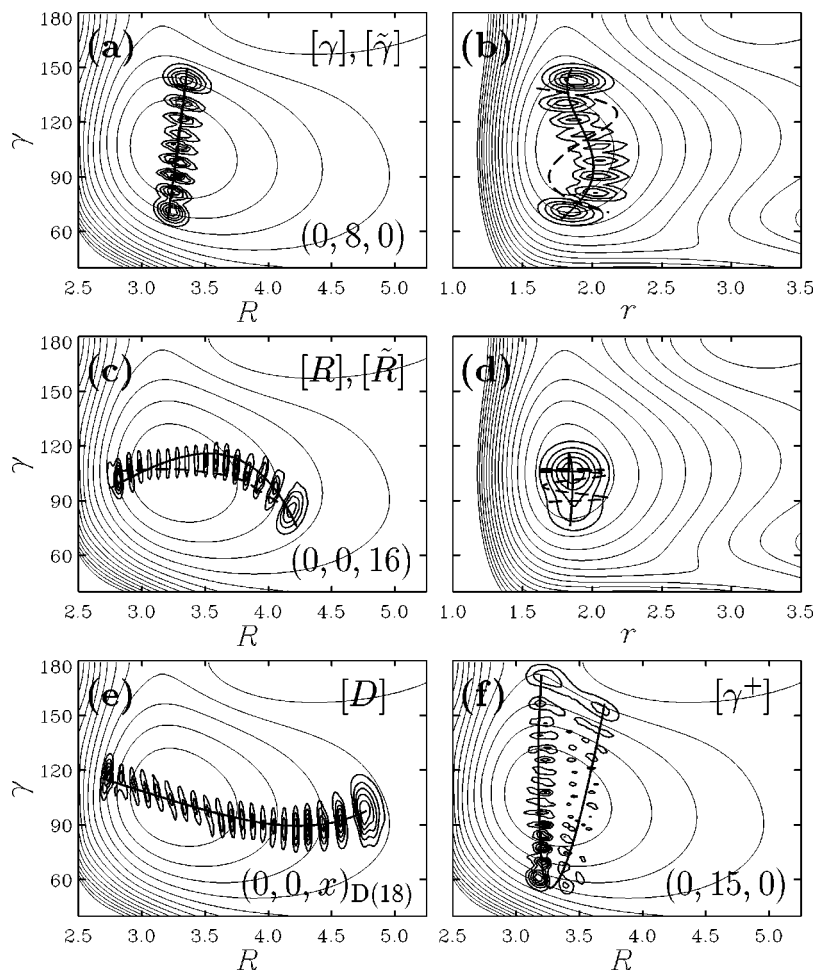
FIG. 11. Comparison of selected POs and the corresponding wave functions (two-dimensional contour plots; the third coordinate is integrated over). (a), (b) The solid (dashed) lines represent orbits of the $[\widetilde{\gamma}]$ ($[\gamma]$) type; (c), (d) the solid (dashed) lines represent orbits of the $[\widetilde{R}]$ ($[R]$) type; (e) the solid line represents an orbit of the $[D]$ type; (f) the solid line shows an orbit of the $[\gamma^+]$ type.

individual POs we present in Fig. 5(d) the corresponding frequencies as functions of the energy (continuation/bifurcation diagram[76]). In order to simplify the presentation, the frequency for the $[r]$ family is not shown. In accordance with the quantum mechanical results in Figs. 5(a)–5(c) the frequencies of the $[\gamma]$-type orbits are divided by two. All classical curves are shifted by 0.23 eV, the estimated quantum mechanical zero-point energy in the HO stretching mode at the equilibrium configuration, to higher energies.[77] Representative examples of POs and the corresponding wave functions are depicted in Fig. 11.

The $[r]$-type POs (not shown) exist up to very high energies, far above threshold, and they are stable for the entire energy regime studied. The general structure of these orbits does not change as energy increases. The behavior of the POs of the other two principal families, however, is more involved.

In contrast to the $[r]$ orbits, the $[\gamma]$-type POs very early change their qualitative morphology: As energy increases the HO mode becomes excited, as is seen in Fig. 11(b) (the dashed line), and the degree of excitation grows with E. These changes start around -1.95 eV (including the 0.23 eV shift to higher energies) and are the consequence of the 3:1 resonance between the HO mode and the bending mode. This resonance has only a small effect on the quantum mechanical wave functions, but seems to influence the classical trajectories more strongly. However, although the $[\gamma]$ family

of POs remains stable up to energies well above the dissociation threshold and although they seem to follow the backbone of the $(0,v_2,0)$ wave functions in the (R,γ) plane [Fig. 11(a)], they do not scar the $(0,v_2,0)$ wave functions: The behavior of the wave functions in the (r,γ) plane [Fig. 11(b)] is not properly described by the $[\gamma]$-type POs.

In the same energy range, where the $[\gamma]$-type POs change their structure (-1.95 eV), the first saddle-node (SN) bifurcation is found. The stable branch of this bifurcation, which is denoted by $[\widetilde{\gamma}]$ in what follows, has POs with small excitation along the r coordinate — for low energies as well as for high energies. As Figs. 11(a) and 11(b) indicate, it is the POs of the $[\widetilde{\gamma}]$ family which scar the $(0,v_2,0)$ wave functions. The $[\widetilde{\gamma}]$ POs are stable up to about -0.4 eV, where a period-doubling bifurcation occurs. At this bifurcation the $[\widetilde{\gamma}]$ branch becomes unstable and the new branch, labeled by $[\gamma^+]$, is stable, at least initially. At still higher energies this branch goes through several additional bifurcations and eventually also loses its stability.

As previously mentioned, the pure bending wave functions $(0,v_2,0)$ change their shapes at high energies, i.e., when v_2 is larger than 13 or so. While at lower energies the $(0,v_2,0)$ wave functions do not have a node in the R direction, in the high-energy regime they develop excitation in R [Fig. 11(f)]. The structural change of the wave functions is reflected by the change of the slope of the

J. Chem. Phys., Vol. 112, No. 1, 1 January 2000

Bifurcations in the spectrum of HOCl   89

$(0,v_2,0)$-frequency curve near -0.25 eV in Fig. 5(c). The high-energy $(0,v_2,0)$ wave functions are scarred by the POs of the $[\gamma^+]$ branch, which have the shape of a very narrow horseshoe [Fig. 11(f)]. Because of the splitting into two branches, the period of the $[\gamma^+]$ orbits is about two times longer than the period of the $[\tilde{\gamma}]$-type POs (period-doubling bifurcation); accordingly, the frequency is lowered by a factor of 2. (Actually, in order to compare with the corresponding quantum mechanical frequency curve, the frequency of the $[\gamma^+]$-type orbits should be multiplied by two.) The horseshoe becomes increasingly wider with increasing energy. At still higher energies these POs also become unstable, which explains why no clear-cut $(0,v_2,0)$ wave functions exist above 0 eV or so.

The POs of the $[R]$-type principal family are also stable up to very high energies. However, there is a sudden change of the frequency around -1.4 eV and at the same time a change of the character of these orbits. While below -1.4 eV the $[R]$-type orbits have no significant excitation in r, above this energy they show substantial excitation in the HO stretching mode [see Fig. 11(d) (dashed lines)], which grows with energy. A careful analysis of the eigenvalues of the monodromy matrix shows that the POs belonging to the two apparently different parts of the frequency curve are members of the same family. The $[R]$-type orbits change abruptly their character. The cause of this transition is the almost exact 1:6 resonance between the r coordinate, which was basically unexcited up to this energy, and R. Above -1.4 eV the additional energy is to a large extent channeled into r motion, while the energy contained in R increases only slightly. Figures 11(c) and 11(d) clearly show that the $(0,0,v_3)$ wave functions do not follow the $[R]$-type POs.

At the energy, where the resonance between R and r sets in, a second SN bifurcation emanates, the stable branch of which will be denoted by $[\tilde{R}]$ in what follows. The orbits belonging to this manifold have the same character as the POs of the $[R]$ family below the SN bifurcation. In particular, they do not have substantial excitation in r and therefore are believed to scar the wave functions of the $(0,0,v_3)$ progression [Figs. 11(c) and 11(d)]. The $[\tilde{R}]$ branch is stable up to the highest energy considered. It seems to be the high-energy continuation of the low-energy branch of the $[R]$ family.

The sudden change of the frequency of the $[R]$ family and the occurrence of the SN bifurcation, at which the $[\tilde{R}]$ orbits are born, is to some extent replicated at higher energies: There is a whole cascade of SN bifurcations. The corresponding trajectories will be denoted by $[D_1]$, $[D_2]$, etc. All frequency curves of the $[D_i]$ families have a similar pattern, that is, a short branch with large anharmonicity, which appears to be the extrapolation of the low-energy segment of the $[R]$ family, and a second part, for which the slope is smaller, approximately the same as for the $[r]$ family. The trajectories belonging to the first branch are stable, have no excitation in r, and scar the $(0,0,x)_{D(P)}$ wave functions, which is the reason why we term them $[D_i]$ orbits. On the other hand, the trajectories belonging to the second segments are mainly unstable, show considerable excitation of

the HO mode, and therefore do not guide the $(0,0,x)_{D(P)}$ wave functions, which do not show excitation along the r coordinate. It is plausible to assume that the abrupt change of the $[R]$ frequency and the corresponding changeover of the morphology of the orbits at the SN bifurcation near -1.4 eV, on the one hand, and the changes of the $[D_i]$ frequency curves and the change of the character of the $[D_i]$-type trajectories, on the other, have the same origin, namely the resonance between r and R. While the former SN bifurcation is the result of a 6:1 resonance, the SN bifurcations of the $[D_i]$ families are caused by 8:1, 9:1 resonances, etc., as the analysis of the unstable trajectories in the (R,r) plane indicates.

It is not surprising that the families of periodic orbits, which are associated with excitation in r, appear at energies at which the r mode tunes into resonance with the other two modes. Of course, a mode which is almost separated from the other two modes classically can be excited at any energy — one simply has to put some amount of energy into r, where it will stay because of the separability. However, the resulting trajectories would be only quasiperiodic rather than fully periodic. A given trajectory is periodic if the number of cycles in the (separable) mode r is a multiple of the number of cycles in the (R,γ) plane and this means that the r mode is in resonance with the other two modes. This explains why the $[R]$ and $[D_i]$ families have SN bifurcations at specific energies. The amount of energy put into the r mode along these special periodic orbits does not correspond to one quantum of HO stretch vibration and therefore quantum mechanics totally ignores these bifurcated branches. A similar situation was previously discussed in Ref. 73 in connection with the PO analysis of HCP.

The classical continuation/bifurcation diagram looks much more complicated than its quantum mechanical counterpart in Fig. 5(c). If only those branches, which apparently correspond to the quantum mechanical curves [highlighted by thicker lines in Fig. 5(d)], were drawn, the analogy between Figs. 5(c) and 5(d) would be more evident. Nevertheless, we also show those branches, which do not affect the quantum mechanical wave functions of the overtone states, because they are the high-energy continuations of those segments which at lower energies do influence the quantum mechanical states. All of these branches have one feature in common, i.e., significant excitation of the HO mode. As a result of this, their anharmonicities are similar to that of the $[r]$ branch. The continuation/bifurcation diagram obtained in the 2D model, in which the HO vibration is *adiabatically* decoupled, is much simpler and resembles very closely the corresponding quantum mechanical picture.[33]

In previous applications of PO analysis to molecular systems[18,78,79] we observed SN bifurcations to occur mainly near energies, where the topography of the potential changes drastically, e.g., near a barrier (HCN[80]) or a ''kink'' (HCP[12]). In these cases, the principal families continue to exist with the corresponding POs gradually changing their morphologies; the new regions of phase space, which become accessible, are explored by the POs of the SN families. HCP is a well-understood example.[13] The situation is different for HOCl. First, the PES does not have a characteristic

feature like a barrier, at least not in the energy regime studied in the present investigation, which underlines that SN bifurcations do not require drastic changes of the PES. Second, at the SN bifurcation the POs of the principal families change drastically by penetrating into a new dimension (r) and the emerging SN orbits explore those regions of phase space which before the SN bifurcation are sampled by the principal families. A more detailed analysis of this development will be published at a later date by investigating a two-dimensional model (coordinates R and γ), in which r is treated as a second control parameter in addition to E.

VI. UNIMOLECULAR DISSOCIATION

In Secs. IV and V we analyzed the evolution of the bound states up to the dissociation threshold and showed how they are affected by SN bifurcations of the classical phase space. In this section we will discuss the implications of the bound-state structure for the fragmentation above the HO+Cl threshold. The link between spectroscopy, on the one hand, and kinetics (i.e., unimolecular dissociation), on the other, are resonances, that is, quasibound states in the dissociation continuum. In scattering theory, resonances emerge as poles of the S matrix.[81] In our calculations, based on Feschbach's optical model, resonances are approximated by the eigenvectors of a complex-symmetric Hamiltonian (see Sec. III). This Hamiltonian differs from the one used in the bound-state calculations by an imaginary absorbing potential term. As such, each resonance is uniquely characterized by a complex wave function and a complex eigenenergy, $E_0 - i\Gamma/2$. The real part determines the position of the resonance on the energy axis (in what follows E_0 is the energy in excess of the dissociation threshold), and the imaginary part gives the resonance width. The resonance lifetime is given by $\tau = \hbar/\Gamma$, and the dissociation rate is defined as $k = \tau^{-1}$.

An overview of the dissociation dynamics of HOCl was already given in Ref. 23, where we calculated (with a different method than the one employed in the present work) the resonance widths in the region from the threshold up to about 4000 cm^{-1} above it. The main finding was a pronounced state dependence of the unimolecular decay with k fluctuating over seven orders of magnitude. A detailed analysis of this wide distribution was not the aim of that initial survey study. In the present work we attempt to rationalize the strong state dependence of the resonance widths and to this end analyze the resonance wave functions and relate their structure to the magnitude of the dissociation rate. For convenience, only a narrow energy range of about 500 cm^{-1} above the threshold is considered. Each of the ~ 160 eigenfunctions is visually inspected and assigned (when possible). A complete list of the calculated resonance energies, widths, and assignments can be obtained from one of the authors (R.S.) or electronically.[70]

The resonances can be roughly divided into two groups: Those whose wave functions are mainly confined to the region of the potential well—with only small amplitudes in the exit channel and those whose wave functions extend far out into the dissociation channel, in many cases even to the boundary of the grid. In order to simplify the notation, we
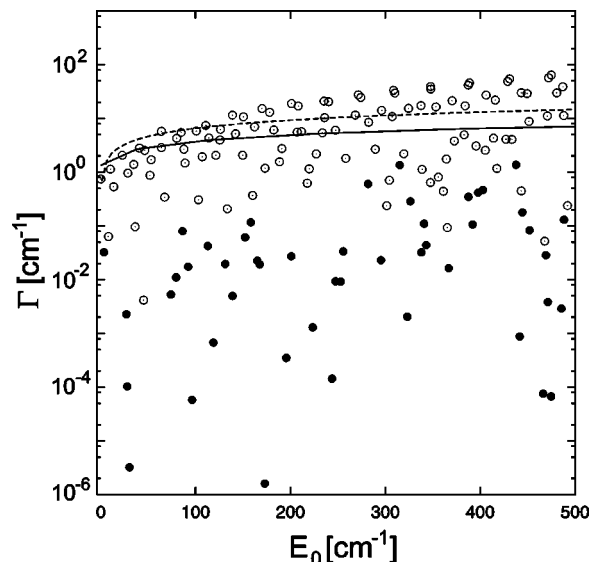

FIG. 12. Resonance widths Γ as a function of the excess energy E_0. The widths for states which are mainly localized in the region of the potential well are represented by the closed circles and the widths for states which extend far into the fragment channel are indicated by the open circles. The solid line is the width estimated from SACM theory and the dashed line represents $\Gamma_{max}(E_0)$ defined in Eq. (13).

will refer to the first group of states as quasibound states and denote the resonances with wave functions significantly penetrating into the product channel as ''d'' states in what follows. The states denoted by $(v_1, v_2, x)_D$ previously are a subgroup of the ''d'' states. The distinction of the two groups is, of course, not completely unambiguous. All calculated resonance widths are depicted in Fig. 12.

Most of the quasibound states have widths below 1 cm^{-1}, which corresponds to a lifetime of the order of 5 ps. Many of them have a clear-cut assignment in terms of quantum numbers (v_1, v_2, v_3) in the same way as the true bound states [Fig. 13(a)]. All assignable states have at least one
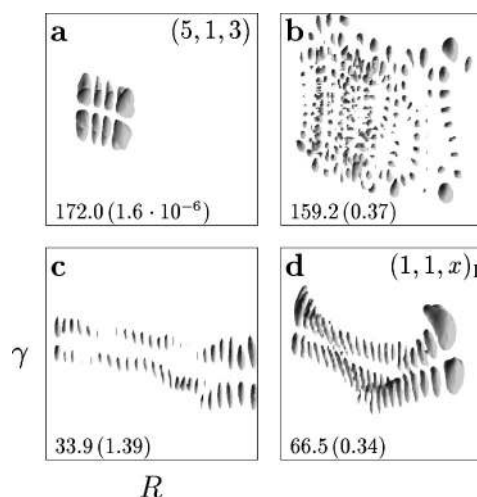

FIG. 13. (a)–(d) Selected examples of resonance wave functions. The γ axis ranges from 19° to 178° and the R axis ranges from $2.5a_0$ to $5.43a_0$. The two numbers in each panel are the excess energy E_0 and the width Γ (in brackets), respectively, both given in cm^{-1}. The wave function in (c) extends far beyond the range shown.

quantum stored in the weakly coupled HO stretching mode. As previously mentioned, the spectra for different values of $v_1 \geq 1$ are to a large extent replicas of the spectrum of $v_1 = 0$. Thus, exciting HO by one or several quanta promotes a considerable number of states with clear–cut assignment into the continuum without making the excess energy directly available for the dissociation mode. In other cases the assignment is not at all clear [Fig. 13(b)]. Such states typically have many quanta in modes 2 and 3 and relatively large widths. The widths of the quasibound states show a great diversity with fluctuations over several orders of magnitude. Because of the very narrow energy interval studied, it is not possible to investigate longer ''progressions'' of resonances like for HCO, for example.[82] Nevertheless, some conclusions can be drawn. The lower bound of the distribution is formed by the states with strong excitation in the HO mode and weak excitation in the other two modes. Their width can be as low as 10^{-6} cm^{-1}. It must be underlined that states with large values of v_3 do not necessarily have large dissociation rates. As previously discussed, the $(0,0,v_3)$ states are strongly bent in the (R, γ) plane, i.e., they avoid the direct dissociation path, and therefore they do not couple efficiently to the continuum. Strongly fluctuating widths for the assignable states have been also reported by Skokov, Bowman, and Mandelshtam[31] in their study of the HOCl dissociation.

The resonances belonging to the ''d'' group must be analyzed with great caution. Since their wave functions extend with large amplitude into the dissociation channel, in many cases they must be interpreted as ''direct scattering states.'' In contrast to the quasibound states, their widths are difficult to converge with respect to the parameters (onset and strength) of the optical potential, especially for those states whose wave functions reach the end of the grid. Because the ''d'' states have strong excitation in the dissociation mode, the widths are generally much larger than the widths of the quasibound states ($\Gamma > 1$ cm^{-1} or so). The reason why we do not eliminate them from the present discussion is their close similarity with the D states discussed in great detail in the previous sections.

A rough estimate of whether a pole of the Green's function represents a meaningful resonance state or not can be derived as follows. The wave number, corresponding to the dissociation mode R, for a complex eigenstate is also complex,[83]

$$k_R = \frac{1}{\hbar} \sqrt{2 \mu_R (E_0 - i\Gamma/2)}. \tag{12}$$

Thus, the outgoing wave, $\exp(ik_R R/\hbar)$, contains an exponentially growing admixture, which for a narrow resonance has the form $\exp[+(\mu_R/8E_0)^{1/2}\Gamma R/\hbar]$. This term becomes significant at a certain ''critical distance,'' $R = R^*$, at which the exponent is of order of unity. R^* is a function of the resonance width and the excess energy E_0: The broader the resonance and the smaller E_0, the smaller is R^*. If R^* lies in the inner part of the potential, the divergent term strongly affects the wave function and an assignment consistent with the assignment of bound states cannot be made. In contrast, wave functions with R^* lying in the asymptotic region can be analyzed as if they were bound. Rigorously speaking, only those

states are undisturbed by the exponential growth for which R^* exceeds the potential radius, that is — in practice — the boundary of the grid, R_{max}. The condition $R^* = R_{max}$ defines a maximum resonance width, which a state may have without being affected by the exponential divergence,

$$\Gamma_{max}(E_0) \approx 2\hbar \sqrt{2E_0/\mu_R} R_{max}^{-1}. \tag{13}$$

The square root in this equation is the velocity v_R of a free particle with mass μ_R and energy E_0, and thus the maximum width corresponds to the time a particle, ballistically ejected, requires to fly across the grid. This estimation suggests that the interpretation of poles with $\Gamma > \Gamma_{max}$ as ''metastable'' states is rather symbolic. For HOCl, a typical value of Γ_{max} close to the threshold ($E_0 = 10$ cm^{-1}) is 2 cm^{-1}, while for 500 cm^{-1} above the threshold $\Gamma_{max} \approx 14$ cm^{-1}. The large reduced mass of the HO–Cl system causes Γ_{max} to be so small in the present case. The curve $\Gamma_{max}(E_0)$ is depicted in Fig. 12; for comparison, the widths according to the statistical adiabatic channel model of Quack and Troe[84] are also shown. Of course, the one-dimensional estimation Eq. (13) is only an upper limit. All the quasibound states have widths, which fulfill the requirement $\Gamma < \Gamma_{max}$. A more rigorous way for distinguishing the real resonance states from direct scattering states would be to perform calculations for different grid boundaries and to analyze how the various pole energies vary. This is a very time consuming procedure and has not been done here.

A typical wave function for a state with $\Gamma \approx \Gamma_{max}$ is depicted in Fig. 13(c). It stretches all the way to the boundary of the grid. Although the HO mode is not excited, it has a regular nodal structure in the R coordinate, and excitation in the local bending mode can be clearly distinguished. Because wave functions of this type are so similar to those shown in Fig. 6 (right column), we believe that these states are the continuations of the bound $(v_1, v_2, v_3)_{D(P)}$ states into the continuum. Their lifetimes are nearly ballistic or even smaller. The D states just under the threshold are kept bound only by a tiny potential force at large interfragment distances. Several wave numbers of additional energy in the dissociation mode are enough to smoothly transform them into quickly dissociating states. A similar effect was recently observed in model studies of the near-threshold dissociation of NO$_2$.[85]

Nevertheless, there are also a few states of the ''d'' type with widths well below Γ_{max} and which can be considered as quasibound states. They have at least one quantum of HO stretch. Because a substantial amount of energy is stored in the weakly coupled mode, their lifetime is comparatively long. These states are bound with respect to the HO($v_1 = 1$) asymptote and can decay only by a nonadiabatic transition to $v_1 = 0$ manifold, in a similar way as previously described for HCO.[86] A wave function for a typical example is shown in Fig. 13(d). Except for a small-amplitude tail it does not extend to the grid boundary and has exactly the form of the $(v_1, v_2, v_3)_{D(P)}$ bound-state wave functions.

The extreme state specificity of HOCl is mainly due to a lack of coupling between the modes. If the coupling were stronger, the dynamics would be more irregular and the wave functions would look — on average — more alike. As a

consequence, the dissociation rates would not vary as much as for HOCl. The dissociations of HNO[21] and NO_2 (Ref. 87) are typical examples.

VII. SUMMARY

(1) We have calculated a potential energy surface for the ground electronic state of HOCl appropriate for studying the dissociation into HO and Cl. The *ab initio* calculations have been performed using the multireference configuration-interaction method and a quintuple-zeta one-particle basis set. The agreement with known experimental data (equilibrium data, dissociation energy, transition frequencies) is very good.

(2) All bound states up to the dissociation threshold, for total angular momentum $J=0$, have been calculated by means of the filter diagonalization technique. Altogether, our potential energy surface supports 827 bound vibrational states.

(3) The bound state spectrum is affected by a 2:1 anharmonic resonance between the HOCl bending mode and the OCl stretching mode leading to a clustering of the energy levels in terms of polyads. The resonance is only approximate at low energies, but because of the anharmonicity of the OCl stretching mode it becomes better and better fulfilled at higher energies.

(4) As a result of the Fermi resonance the bending mode and the OCl stretching mode are significantly mixed with the consequence that the pure $(0,0,v_3)$ overtone states acquire more and more bending character and avoid the dissociation channel.

(5) States, which do clearly follow the dissociation path, come into existence at high energies. This family of states is very anharmonic with the result that their density quickly increases with energy.

(6) The structure of the quantum mechanical spectrum and the quantum mechanical wave functions has been interpreted in terms of the structure of the classical phase space and certain stable periodic orbits. In particular, the abrupt birth of the dissociation states can be viewed as the result of a saddle-node or tangent bifurcation.

(7) The bound-state spectrum persists into the continuum with the wide variety of wave function structures leading to a pronounced state specificity of the dissociation rates. The above-threshold counterparts of the bound states with clear extension along the dissociation channel are broad resonances with nearly ballistic lifetimes.

ACKNOWLEDGMENTS

Note added in proof. A similar study of the bound-state spectrum of HOCl has been performed by R. Jost *et al.* [J. Chem. Phys. **111**, 6807 (1999)].

[1] *Molecular Dynamics and Spectroscopy by Stimulated Emission Pumping*, edited by H.-L. Dai and R. W. Field (World Scientific, Singapore, 1995).
[2] E. B. Wilson, J. C. Decius, and P. C. Cross, *Molecular Vibrations* (McGraw-Hill, New York, 1954).
[3] M. J. Davis, Int. Rev. Phys. Chem. **14**, 15 (1995).
[4] M. E. Kellman, Int. J. Quantum Chem. **65**, 399 (1997).
[5] D. Papousek and M. R. Aliev, *Molecular Vibrational-Rotational Spectra* (Elsevier, Amsterdam, 1982).
[6] C. C. Martens and G. S. Ezra, J. Chem. Phys. **86**, 279 (1987).
[7] M. E. Kellman, in Ref. 1.
[8] M. E. Kellman, Annu. Rev. Phys. Chem. **46**, 395 (1995).
[9] M. Joyeux, Chem. Phys. **203**, 281 (1996).
[10] H.-M. Keller, T. Schröder, M. Stumpf, C. Stöck, F. Temps, R. Schinke, H.-J. Werner, C. Bauer, and P. Rosmus, J. Chem. Phys. **106**, 5359 (1997).
[11] H. D. Mordaunt, H. Flöthmann, M. Stumpf, H.-M. Keller, C. Beck, R. Schinke, and K. Yamashita, J. Chem. Phys. **107**, 6603 (1997).
[12] C. Beck, H.-M. Keller, S. Yu. Grebenshchikov, R. Schinke, S. C. Farantos, K. Yamashita, and K. Morokuma, J. Chem. Phys. **107**, 9818 (1997).
[13] H. Ishikawa, R. W. Field, S. C. Farantos, M. Joyeux, J. Koput, C. Beck, and R. Schinke, Annu. Rev. Phys. Chem. **50**, 443 (1999).
[14] M. C. Gutzwiller, *Chaos in Classical and Quantum Mechanics* (Springer, New York, 1990).
[15] J. Guckenheimer and P. Holmes, *Nonlinear Oscillations, Dynamical Systems, and Bifurcations of Vector Fields* (Springer, Berlin, 1983).
[16] H. Ishikawa, C. Nagao, N. Mikami, and R. W. Field, J. Chem. Phys. **106**, 2980 (1997).
[17] J. M. Gomez Llorente and E. Pollak, Annu. Rev. Phys. Chem. **43**, 91 (1992).
[18] S. C. Farantos, Int. Rev. Phys. Chem. **15**, 345 (1996).
[19] S. C. Farantos, Comput. Phys. Commun. **108**, 240 (1998).
[20] R. Schinke, *Photodissociation Dynamics* (Cambridge University Press, Cambridge, 1993).
[21] R. Schinke, C. Beck, S. Yu. Grebenshchikov, and H.-M. Keller, Ber. Bunsenges. Phys. Chem. **102**, 593 (1998).
[22] J. M. Bowman, J. Phys. Chem. A **102**, 3006 (1998).
[23] J. Hauschildt, J. Weiß, S. Yu. Grebenshchikov, R. Düren, R. Schinke, and J. Koput, Chem. Phys. Lett. **300**, 569 (1999).
[24] B. Abel, H. H. Hamann, A. A. Kachanov, and J. Troe, J. Chem. Phys. **104**, 3189 (1996).
[25] B. Abel, A. Charvát, S. F. Deppe, and H. H. Hamann, Ber. Bunsenges. Phys. Chem. **101**, 329 (1997).
[26] R. J. Barnes, G. Dutton, and A. Sinha, J. Phys. Chem. **101**, 8374 (1997).
[27] R. J. Barnes and A. Sinha, J. Chem. Phys. **107**, 3730 (1997).
[28] M. R. Wedlock, R. Jost, and T. R. Rizzo, J. Chem. Phys. **107**, 10344 (1997).
[29] S. Skokov, K. A. Peterson, and J. M. Bowman, J. Chem. Phys. **109**, 2662 (1998).
[30] S. Skokov, J. Qi, J. M. Bowman, C.-Y. Yang, S. K. Gray, K. A. Peterson, and V. A. Mandelshtam, J. Chem. Phys. **109**, 10273 (1998).
[31] S. Skokov, J. M. Bowman, and V. A. Mandelshtam, Phys. Chem. Chem. Phys. **1**, 1279 (1999).
[32] S. Skokov and J. M. Bowman, J. Chem. Phys. **110**, 9789 (1999).
[33] S. Yu. Grebenshchikov, R. Schinke, and M. Joyeux (unpublished).
[34] H.-J. Werner and P. J. Knowles, J. Chem. Phys. **89**, 5803 (1988).
[35] P. J. Knowles and H.-J. Werner, Chem. Phys. Lett. **145**, 514 (1988).
[36] T. H. Dunning, Jr., J. Chem. Phys. **90**, 1007 (1989).
[37] D. E. Woon and T. H. Dunning, Jr., J. Chem. Phys. **98**, 1358 (1993).
[38] H.-J. Werner and P. J. Knowles, J. Chem. Phys. **82**, 5053 (1985).
[39] P. J. Knowles and H.-J. Werner, Chem. Phys. Lett. **115**, 259 (1985).
[40] S. R. Langhoff and E. R. Davidson, Int. J. Quantum Chem. **8**, 61 (1974).
[41] E. R. Davidson and D. W. Silver, Chem. Phys. Lett. **52**, 403 (1978).
[42] MOLPRO-96 is a package of *ab initio* programs written by H.-J. Werner and P. J. Knowles, with contributions from J. Almlöf, R. D. Amos, M. J. O.

Deegan, S. T. Elbert, C. Hampel, W. Meyer, K. A. Peterson, R. Pitzer, A. J. Stone, P. R. Taylor, R. Lindh, M. E. Mura, and T. Thorsteinsson.

[43] R. Schinke, J. Chem. Phys. **80**, 5510 (1984).

[44] A. Laganá, G. O. de Aspuru, and E. Garcia, J. Chem. Phys. **108**, 3886 (1998).

[45] K. S. Sorbie and J. N. Murrell, Mol. Phys. **29**, 1387 (1975).

[46] B. R. Johnson and N. W. Winter, J. Chem. Phys. **66**, 4116 (1977).

[47] W. H. Press, S. A. Teukolsky, W. T. Vetterling, and B. P. Flannery, *Numerical Recipies in Fortran: The Art of Science Computing* (Cambridge University Press, Cambridge, 1992).

[48] C. M. Deeley, J. Mol. Spectrosc. **122**, 481 (1987).

[49] R. M. Escribano, D. Di Lonardo, and L. Fusina, Chem. Phys. Lett. **259**, 614 (1996).

[50] J. S. Wells, R. L. Sams, and W. J. Lafferty, J. Mol. Spectrosc. **77**, 349 (1979).

[51] W. J. Lafferty and W. B. Olson, J. Mol. Spectrosc. **120**, 359 (1986).

[52] C. M. Deeley and I. M. Mills, J. Mol. Spectrosc. **114**, 368 (1985).

[53] C. Azzolini, F. Cavazza, G. Crovetti, G. Di Lonardo, R. Frulla, R. Escribano, and L. Fusina, J. Mol. Spectrosc. **168**, 494 (1994).

[54] F. Cavazza, G. Di Lonardo, R. Escribano, L. Fusina, P. G. Gomez, and J. Ortigoso, J. Mol. Spectrosc. **159**, 395 (1993).

[55] A. Charvát, S. F. Deppe, H. H. Hamann, and B. Abel, J. Mol. Spectrosc. **185**, 336 (1997).

[56] H. H. Hamann, A. Charvát, B. Abel, S. A. Kovalenko, and A. A. Kachanov, J. Chem. Phys. **106**, 3103 (1997).

[57] K. A. Peterson, Spectrochim. Acta B **53**, 1051 (1997).

[58] J. Koput and K. A. Peterson, Chem. Phys. Lett. **283**, 139 (1998).

[59] M. R. Wall and D. Neuhauser, J. Chem. Phys. **102**, 8011 (1995).

[60] V. A. Mandelshtam and H. S. Taylor, J. Chem. Phys. **102**, 7390 (1995).

[61] T. P. Grozdanov, V. A. Mandelshtam, and H. S. Taylor, J. Chem. Phys. **103**, 7990 (1995).

[62] R. Kosloff, Annu. Rev. Phys. Chem. **45**, 145 (1994).

[63] V. A. Mandelshtam, T. P. Grozdanov, and H. S. Taylor, J. Chem. Phys. **103**, 10074 (1995).

[64] V. A. Mandelshtam and H. S. Taylor, J. Chem. Soc., Faraday Trans. **93**, 847 (1997).

[65] J. Echave and D. C. Clary, Chem. Phys. Lett. **190**, 225 (1992).

[66] Z. Bačić and J. C. Light, Annu. Rev. Phys. Chem. **40**, 469 (1989).

[67] G. Jolicard and E. J. Austin, Chem. Phys. Lett. **121**, 106 (1985).

[68] G. Jolicard and E. J. Austin, Chem. Phys. **103**, 295 (1986).

[69] U. V. Riss and H.-D. Meyer, J. Phys. B **24**, 4503 (1993).

[70] See EPAPS Document No. E-JCPSA-6-112-009001 for a complete list of calculated bound-state and resonance energies, widths, and assignments. This document may be retrieved via the EPAPS homepage (http://www.aip.org/pubservs/epaps.html) or from ftp.aip.org in the directory /epaps/. See the EPAPS homepage for more information.

[71] D. W. Noid, M. L. Koszykowski, and R. A. Marcus, J. Chem. Phys. **71**, 2864 (1979).

[72] J. Svitak, Z. Li, J. Rose, and M. E. Kellman, J. Chem. Phys. **102**, 4340 (1995).

[73] M. Joyeux, S. Yu. Grebenshchikov, and R. Schinke, J. Chem. Phys. **109**, 8342 (1998).

[74] H. S. Taylor, in Ref. 1.

[75] E. J. Heller and S. Tomsovic, Phys. Today **46**, 38 (1993).

[76] G. Contopoulos, Astron. J. **75**, 96 (1970).

[77] A more correct treatment would also include the zero-point energy in the other two degrees of freedom, i.e., the zero-point energy in the bending mode for the [R] branch and *vice versa*, the zero-point energy in the R mode for the [γ] branch. However, these energies are about a factor of 3 and 6 smaller than the zero-point energy in the HO stretching mode and therefore neglected.

[78] L. Zachilas and S. C. Farantos, Chem. Phys. **154**, 55 (1991).

[79] R. Prosmiti, S. C. Farantos, R. Guantes, F. Borondo, and R. M. Benito, J. Chem. Phys. **104**, 2921 (1996).

[80] S. C. Farantos and M. Founargiotakis, Chem. Phys. **142**, 345 (1990).

[81] L. D. Landau and E. M. Lifschitz, *Quantum Mechanics. Non-Relativistic Theory* (Pergamon, New York, 1976).

[82] H.- M. Keller, H. Flöthman, A. J. Dobbyn, R. Schinke, H. -J. Werner, C. Bauer, and P. Rosmus, J. Chem. Phys. **105**, 4983 (1996)

[83] E. Merzbacher, *Quantum Mechanics* (Wiley, New York, 1970).

[84] M. Quack and J. Troe, Ber. Bunsenges. Phys. Chem. **78**, 240 (1974).

[85] S. Yu. Grebenshchikov, A. Delon, R. Schinke, and R. Jost (unpublished).

[86] H.-J. Werner, C. Bauer, P. Rosmus, H.-M. Keller, M. Stumpf, and R. Schinke, J. Chem. Phys. **102**, 3593 (1995).

[87] S. Yu. Grebenshchikov, R. Schinke, and V. A. Mandelshtam (unpublished).